Available online at www.eccomasproceedia.org
Eccomas Proceedia UNCECOMP (2023) 25-38

ECCOMAS
Proceedia

UNCECOMP 2023
5th ECCOMAS Thematic Conference on
Uncertainty Quantification in Computational Science and Engineering
M. Papadrakakis, V. Papadopoulos, G. Stefanou (eds.)
Athens, Greece, 12-14 June 2023

RESPONSE RECONSTRUCTION IN BRIDGES USING ON-BOARD MEASUREMENTS FROM PASSING VEHICLES

Filippos Filippitzis[1], Ho Man Siu[2], Charikleia Stoura[3], Costas Papadimitriou[1], Elias G. Dimitrakopoulos[2]

[1]University of Thessaly
Department of Mechanical Engineering
Pedion Areos, Volos 38334
e-mail: {fifilipp, costas}@uth.gr

[2]The Hong Kong University of Science and Technology
Department of Civil and Environmental Engineering
Clear Water Bay, Kowloon, Hong Kong, China
e-mail: hmsiu@connect.ust.hk, ilias@ust.hk

[3]ETH Zürich
Institute of Structural Engineering, Department of Civil, Environmental and Geomatic Engineering
Stefano-Franscini-Platz 5, 8093, Zrich, Switzerland
e-mail: charikleia.stoura@ibk.baug.ethz.ch

Abstract. *This work addresses the concept of virtual sensing (response reconstruction) in bridges using information from sensors installed on specially-designed vehicles with known dynamic properties when crossing a bridge. The vehicle and bridge dynamics are coupled through the contact forces at the interface between the two subsystems. The estimation of contact forces employs only the vehicle subsystem (vehicle model and information from sensors installed on the vehicle) and relies on an Augmented Kalman Filter (AKF) technique. Interestingly, the estimated contact forces depend on the characteristics of the rail/road profile irregularities. This work presents a proof of concept using simplified two-degree-of-freedom vehicle models. The bridge model adopted is a simply supported Euler-Bernoulli beam. This simplified analysis provides valuable insight into the effect of different parameters on the accuracy of contact force. The demonstration and proof-of-concept are performed using simulated data from a vehicle-bridge interaction model, considering measurement error and accounting for the effect of irregularities.*

Keywords: On-board sensing, virtual sensing, bridges, fatigue, input-state estimation, response reconstruction.

ISSN:2623-3339
Peer-review under responsibility of the organizing committee of UNCECOMP 2023.
doi: 10.7712/120223.10322.20017

1 INTRODUCTION

Traditional monitoring and identification techniques of bridges rely on sensors installed on the target bridge [1]. An alternative approach to extract information about the structural health of bridges is from on-board sensors mounted on vehicles [2], named vehicle scanning of bridges [3] or indirect bridge identification [4, 5, 6]. Vehicle scanning could potentially provide a rapid and scalable diagnostic approach, without the time-consuming and labour-intensive installation and maintenance of fixed sensor systems.

Vehicle scanning has been proposed to extract a variety of information about bridges. To identify bridge frequencies, Yang and his coworkers investigated the use of the Fourier spectrum to vehicle acceleration [2, 7], contact point response [8, 9], and residual contact point response [10, 11]. They concluded that the contact point response is effective for extracting higher bridge frequencies as it contains no vehicle frequencies. Very recently, Erduran et al. [12] attempted to identify the frequencies of a railway bridge from the acceleration record on the bogies by performing a continuous wavelet transform. Jin et al. [13, 14] proposed a different method to estimate bridge frequencies from on-board sensors, utilizing Stochastic Subspace Identification and processing the vehicle response from two passes in order to eliminate the blurring effect from road roughness. Beyond modal frequencies, Malekjafarian and OBrien focused on estimating mode shapes of bridges from vehicle acceleration measurements by means of a Short Time Frequency Domain Decomposition [15] and Hilbert Huang Transform [16]. Zhou et al. [17] proposed and experimentally tested a two-peak spectrum idealized filter technique for extracting both modal frequencies and mode shapes. Utilizing convex optimization techniques, Eshkevari et al. [18, 19] attempted to identify modal information, including modal frequencies, modal damping ratio, and mode shapes using mobile sensor networks.

In addition to modal information, various indirect identification techniques, including neural network algorithms [20, 21] and different Kalman filters, have been explored to estimate also the road [22, 23, 24, 25] or rail [26] roughness profiles. Zeng et al. [22] proposed a Kalman Filter-based method to calculate the road roughness from a car's tire pressure. Xiao et al.[26] employed a recursive Bayesian Kalman filtering (RBKF) algorithm for estimating the track irregularities and bridge natural frequencies from the vehicle response measurement. Zhao et al. [23, 24] and He and Yang [25] attempted to estimate road roughness from vehicle response measurements with the aid of different variants of Kalman Filters.

Overall, there is growing evidence that vehicle scanning can provide efficient estimation of bridge information and road roughness, which are useful indicators to determine the health status of a bridge structure. To monitor stresses and evaluate fatigue though, it is necessary to reconstruct the bridge response. To this end, the unknown contact force estimation could be essential, which involves solving an unknown input identification problem [27, 28, 29]. Through the use of an Extended Kalman Filter (EKF), Chen et al. [30] estimated the contact force resulting from vehicle-bridge interaction from tire pressure measurements. Wang et al. [31] used an Augmented Kalman Filter (AKF) to estimate the tire force using the measurement of road vehicle responses. These models [30, 31] assumed a viscoelastic contact for the vehicle, which is mainly applicable to road vehicles.

This research examines the use of AKF to estimate the contact force of vehicles with rigid wheels, assuming a rigid contact between the vehicles and the bridge. Numerical case studies are examined using artificial data obtained from the finite element model of a vehicle-bridge system to demonstrate the effectiveness and performance of the approach in contact force estimation and bridge response reconstruction.

2 VEHICLE BRIDGE SYSTEM MODELLING

Consider a vehicle moving along the bridge at a constant speed v. We can model the vehicle as a multi-degree-of-freedom (MDOF) multi-body system, and the bridge as an MDOF Euler-Bernoulli beam (Figure 1). The time-varying contact force vector $\underline{\lambda}(t)$ between the rails is coupling the dynamics of the two sub-systems.

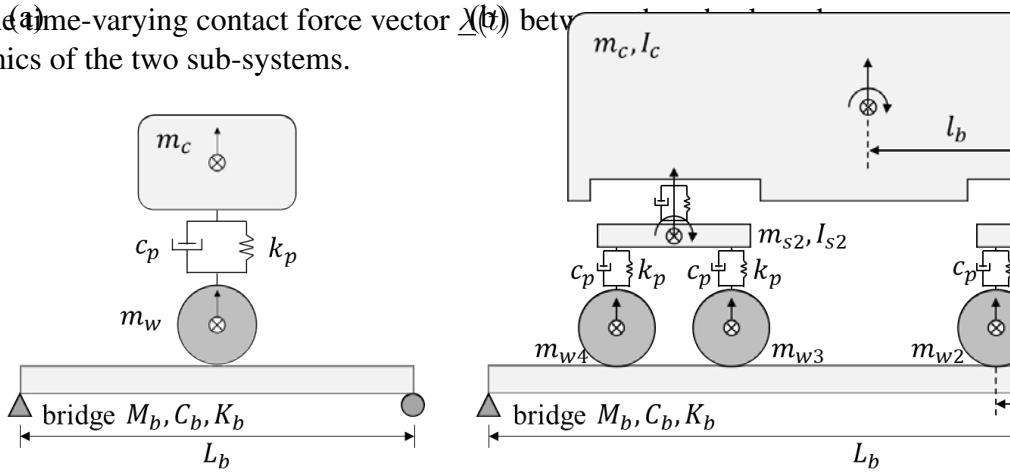

Figure 1: 2-DOF vehicle model on a bridge.

The equation of motion (EOM) of the vehicle sub-system can take the form:

$$M_v\ddot{\underline{u}}_v(t) + C_v\dot{\underline{u}}_v(t) + K_v\underline{u}_v(t) - W_v\underline{\lambda}(t) = \underline{f}_v \tag{1}$$

where, $\underline{u}_v(t)$ is the displacement vector of the vehicle and M_v, C_v, and K_v are, respectively, the mass, damping, and stiffness matrices of the vehicle (subscript $()_v$ denotes the vehicle sub-system). W_v is a contact direction matrix of the vehicle, which maps the contact forces to the contact degrees of freedom (DOFs) of the wheels [32, 33].

Similar to the vehicle subsystem, the EOM of the bridge about its (statically) deformed configuration under its self-weight is:

$$M_b\ddot{\underline{u}}_b(t) + C_b\dot{\underline{u}}_b(t) + K_b\underline{u}_b(t) + W_b\underline{\lambda}(t) = \underline{f}_b \tag{2}$$

with $\underline{u}_b(t)$ being the displacement vector of the bridge and M_b, C_b, and K_b being the mass, damping, and stiffness matrices of the bridge (subscript $()_b$ denotes the bridge subsystem). W_b is a contact direction matrix of the bridge mapping the contact force to the bridge's DOFs [32, 33].

Combining Eqs. (1) and (2), the EOM of the coupled vehicle-bridge system becomes:

$$M\ddot{\underline{u}}(t) + C\dot{\underline{u}}(t) + K\underline{u}(t) + W_c\underline{\lambda}(t) = \underline{f} \tag{3}$$

where, $\underline{u}^T = [\underline{u}_v \;\; \underline{u}_b]$ is the displacement vector of the whole system and M, C, and K are, respectively, the mass, damping, and stiffness matrices of the whole system:

$$M = \begin{bmatrix} M_v & 0 \\ 0 & M_b \end{bmatrix}, C = \begin{bmatrix} C_v & 0 \\ 0 & C_b \end{bmatrix}, K = \begin{bmatrix} K_v & 0 \\ 0 & K_b \end{bmatrix} \tag{4}$$

and $W_c = \begin{bmatrix} -W_v{}^{\mathrm{T}} & W_b{}^{\mathrm{T}} \end{bmatrix}^{\mathrm{T}}$ is the contact direction matrix of the coupled system.

In this study, we assume continuous (i.e., there is no detachment) rigid contact between the wheel and the bridge. This implies a zero relative displacement $\underline{g}_N(x,t) = 0$, velocity

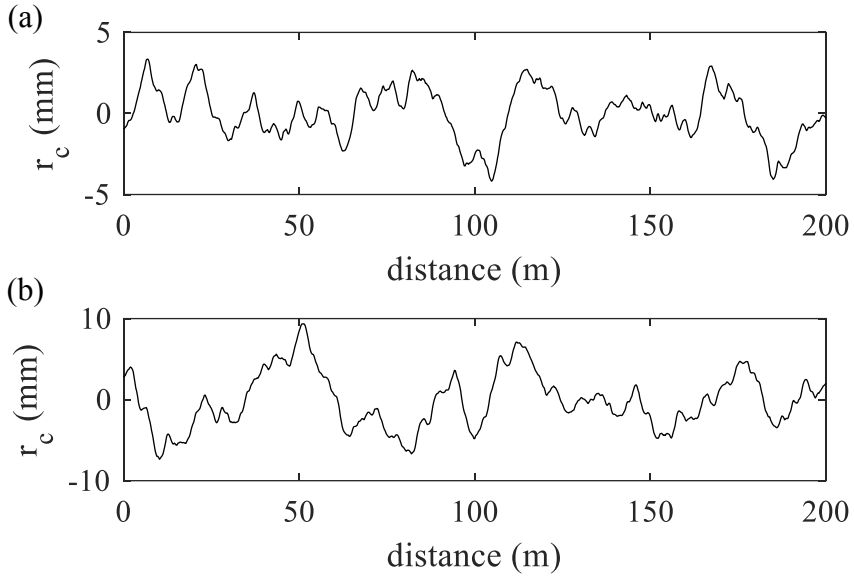

Figure 2: Sample profiles of (a) "very good" quality (b) "good" quality irregularities according to the German spectra for high-speed railway [36].

The explicit expression for the contact force, based on the assumption of rigid contact is:

$$\underline{\lambda} = -G^{-1}[{W_c}^{\mathrm{T}} M^{-1}(\underline{f} - C\underline{\dot{u}}(t) - K\underline{u}(t)) + 2v{W_c}'^{\mathrm{T}}\underline{\dot{u}}(t) + v^2{W_c}''^{\mathrm{T}}\underline{u}(t) - v^2\underline{r_c}''] \tag{6}$$

where G^{-1} is the contact (coupling) mass between the bridge and the vehicle's wheels. The inverse of the coupling mass is written as:

$$G = {W_c}^{\mathrm{T}} M^{-1} W_c. \tag{7}$$

Lastly, in this study, we employ the Newmark-β method to solve the coupled equation.

3 MODAL FORMULATION OF VEHICLE MODEL

To proceed with the Augmented Kalman filtering (AKF) technique for contact force estimation, we employ mode superposition to describe the dynamics of the vehicle. The vehicle model contains at least one zero-frequency mode (i.e., rigid body mode), which is separated from the flexible (deformation) modes. To this end, we partition the mass-normalized mode shape matrix to $\Phi = [\Phi_{rigid}, \Phi_{flex}]$, where Φ_{rigid} contains the mode shape(s) of all m_0 zero-frequency rigid body modes and Φ_{flex} contains the mode shape(s) of all m_f flexible modes ($m_f = m - m_0$) Thus, the relationship between physical and modal coordinates becomes:

$$\underline{u}_v(t) = \underline{u}_s + \underline{u}_d(t) = \underline{u}_s + \Phi\underline{\xi}(t) \tag{8}$$

with $\underline{u}_s$ being the deformed (static) shape of the vehicle due to its self-weight and $\underline{u}_d = \Phi\underline{\xi}(t)$ contributing the time-varying nature of the contact forces λ. Next, the modal displacement vector can be partitioned to $\underline{\xi} = [\underline{\xi}_{rigid}^{\mathrm{T}}, \underline{\xi}_{flex}^{\mathrm{T}}]^{\mathrm{T}}$, where $\underline{\xi}_{rigid}$ and $\underline{\xi}_{flex}$ contain the modal displacement of the rigid body mode(s) and the flexible modes respectively. Substituting Eq. (8) into Eq. (1) and pre-multipling both side by Φ^{T} yields the EOM of the vehicle in modal coordinates:

$$\ddot{\underline{\xi}}_{rigid} = \Phi_{rigid}^{\mathrm{T}} W_v \underline{\lambda}(t) \tag{9}$$

$$\ddot{\underline{\xi}}_{flex} + Z_{flex}\dot{\underline{\xi}}_{flex} + \Lambda_{flex}\underline{\xi}_{flex} = \Phi_{flex}^{\mathrm{T}} W_v \underline{\lambda}(t) \tag{10}$$

where $Z_{flex} = \Phi_{flex}^{\mathrm{T}} C_v \Phi_{flex}$ and $\Lambda_{flex} = \Phi_{flex}^{\mathrm{T}} K_v \Phi_{flex}$.

4 CONTACT FORCE ESTIMATION USING MEASUREMENTS ON VEHICLE

4.1 State-space model of the vehicle in modal coordinates

In time state-space form Equation (10) becomes:

$$\dot{\underline{x}}(t) = A_c \underline{x}(t) + B_c \underline{\lambda}(t) \tag{11}$$

with $\underline{x}(t) = [\underline{\xi}_{flex}^{\mathrm{T}}, \dot{\underline{\xi}}_{flex}^{\mathrm{T}}]^{\mathrm{T}}$ being the state vector, and A_c and B_c being the system matrix and input matrix of the vehicle:

$$A_c = \begin{bmatrix} 0 & I \\ -\Lambda_{flex} & -Z_{flex} \end{bmatrix}, B_c = \begin{bmatrix} 0 \\ \Phi_{flex} W_v \end{bmatrix} \tag{12}$$

Under the assumption of zero-order hold (ZOH), the discrete-time system with a sampling rate $1/\Delta t$ is:

$$\underline{x}_{k+1} = A_d \underline{x}_k + B_d \underline{\lambda}_k + \underline{w}_k \tag{13}$$

with state vector $\underline{x}_k \equiv x(k\Delta t)$, contact force $\underline{\lambda}_k \equiv \lambda(k\Delta t)$, $A_d = e^{A_c \Delta t}$ and $B_d = (A_d - I)A_c^{-1}B_c$ for non-singular A_c. Assume the process noise $\underline{w}_k$ follows a zero-mean Gaussian distribution $\underline{w}_k \sim \mathcal{N}(\underline{0}, Q_x)$ with process noise covariance $Q_x \in \mathbb{R}^{2m_f \times 2m_f}$.

The corresponding observation equation for N_0 measurement quantities is:

$$\underline{y}_k = G\underline{x}_k + J\underline{\lambda}_k + \underline{v}_k \tag{14}$$

where the measurement error term $\underline{v}_k$ is a white noise, i.e. $\underline{v}_k \sim \mathcal{N}(\underline{0}, Q_y)$, with measurement error covariance $Q_y \in \mathbb{R}^{N_0 \times N_0}$.

4.2 AKF for unknown contact force estimation

To model the unknown contact force $\underline{\lambda}_k = \underline{\lambda}(k\Delta t)$ acting on the wheels of the vehicle, we employ a random walk model to allow changes in contact force at different time steps:

$$\underline{\lambda}_{k+1} = \underline{\lambda}_k + \underline{\eta}_k \tag{15}$$

where $\underline{\eta}_k \sim \mathcal{N}(\underline{0}, Q_\lambda)$ is a zero-mean Gaussian prediction error with covariance matrix $Q_\lambda \in \mathbb{R}^{n_\lambda \times n_\lambda}$. By introducing the augmented state vector $\underline{x}_k^a = [\underline{x}_k^{\mathrm{T}}, \underline{\lambda}_k^{\mathrm{T}}]^{\mathrm{T}}$ (consider the contact force

as a part of the state variables of the system), the augmented state-space model and observation equations are formulated as follows:

$$\begin{aligned} \underline{x}^a_{k+1} &= A^a \underline{x}^a_k + \underline{\zeta}_k \\ \underline{y}_k &= G^a \underline{x}^a_k + \underline{v}_k \end{aligned} \tag{16}$$

where the augmented system matrix $A^a \in \mathbb{R}^{(2m_f+n_\lambda)\times(2m_f+n_\lambda)}$ and observation matrix $G^a \in \mathbb{R}^{N_0\times(2m_f+n_\lambda)}$ are:

$$A^a = \begin{bmatrix} A_d & B_d \\ 0 & I \end{bmatrix}, \quad G^a = \begin{bmatrix} G & J \end{bmatrix} \tag{17}$$

while the augmented process noise covariance matrix $Q_a \in \mathbb{R}^{(m_f+n_\lambda)\times(m_f+n_\lambda)}$ of the zero-mean Gaussian white noise sequence $\underline{\zeta}_k \sim \mathcal{N}(\underline{0}, Q_a)$ is:

$$Q_a = \begin{bmatrix} Q_x & 0 \\ 0 & Q_\lambda \end{bmatrix} \tag{18}$$

Through the standard Kalman Filter approach, we can estimate the augmented state vector, which provides the augmented state estimation $\underline{\hat{x}}^a_{k|k}$ and the error covariance matrix $P_{k|k} \in \mathbb{R}^{(2m_f+n_\lambda)\times(2m_f+n_\lambda)}$ obtained using the following time update step:

$$\begin{aligned} \underline{\hat{x}}^a_{k|k-1} &= A^a \underline{\hat{x}}^a_{k-1|k-1} \\ P_{k|k-1} &= A^a P_{k-1|k-1} (A^a)^{\mathrm{T}} + Q_a \end{aligned} \tag{19}$$

and measurement update step:

$$\begin{aligned} K_k &= P_{k|k-1} (G^a)^{\mathrm{T}} (G^a P_{k|k-1} (G^a)^{\mathrm{T}} + Q_y)^{-1} \\ \underline{\hat{x}}^a_{k|k} &= \underline{\hat{x}}^a_{k|k-1} + K_k (\underline{y}_k - G^a \underline{\hat{x}}^a_{k|k-1}) \\ P_{k|k} &= P_{k|k-1} - K_k G^a P_{k|k-1} \end{aligned} \tag{20}$$

5 NUMERICAL EXAMPLES

To evaluate the performance of the proposed Augmented Kalman Filter (AKF), we employ artificial data from (railway) bridge-vehicle interaction simulations. In the following examples, the vehicle enters the bridge at $t = 1$s and moves along a 30 m long simply supported bridge modeled with Euler-Bernoulli beams. Table 1 shows the mechanical properties of the bridge [35].

Table 1: Mechanical properties of the simply supported bridge.

L_b (m)	mass per unit length μ (t/m)	flexural rigidity EI (GNm^2)	damping ratio ζ_b
30	41.74	221.48	2%

Table 2: Mechanical properties of the 2-DOF vehicle.

m_c (t)	m_w (kg)	k_p (MN/m)	c_p (Ns/m)
5.75	1	1.595	126.3

5.1 2 DOFs vehicle with small wheel mass on a smooth rail

To verify the method, this section studies a simplified 2 DOFs vehicle with a small wheel mass moving on the bridge with constant speed $v = 100$km/h. The rail profile is smooth by assumption (i.e., there is no irregularity). Table 2 shows the mechanical properties of the 2-DOF vehicle.

The covariance of the state error is $Q_x = 10^{-8}I$, where I is an identity matrix. The diagonal elements of the covariance matrix Q_y of the measurement error are 10^{-4} times the mean square value of the measured response time history, which corresponds to 1% of the root mean square of the measured response time history. The choice of the covariance of the matrix Q_λ for the random walk model is based on an L-curve analysis [27].

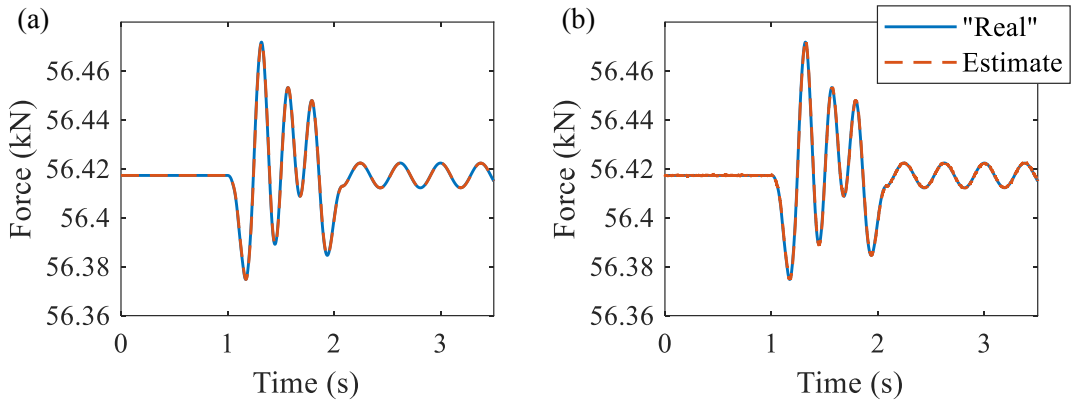

Figure 3: Comparison between the "real" and estimated contact force using the car body acceleration and suspension strain measurement (a) without measurement noise and (b) with 5% measurement noise ($v = 100$km/h).

Figure 3 compares the "real" contact force with the contact force estimated using the car body acceleration and suspension strain measurement with (Figure 3b) and without (Figure 3a) 5% measurement noise. Note that throughout this study "real" indicates the response from the vehicle-bridge simulation. Figure 3a shows that the estimated contact force is identical to the "real" contact force when there is no measurement noise. When there is a 5% measurement noise in the measurement, AKF can still provide a reliable estimation of the contact force.

Figure 4 compares again the "real" and estimated contact forces, but unlike Figure 3, it only uses the car body acceleration with (Figure 4b) and without (Figure 4a) 5% measurement noise. Even in the absence of strain measurement, the estimated contact force matches the "real" contact force when there is no measurement noise. With the introduction of a 5% measurement noise on the measurement, AKF can still provide a reliable estimation of the contact force.

To demonstrate the capability of AKF to reconstruct the contact forces for higher vehicle speeds (i.e., a speed that is closer to the actual operating speed of contemporary trains), we increase the vehicle speed to $v = 250$km/h. Figure 5 compares the "real" and estimated contact

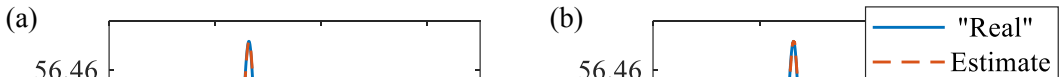

ar body

e0, 250km/h

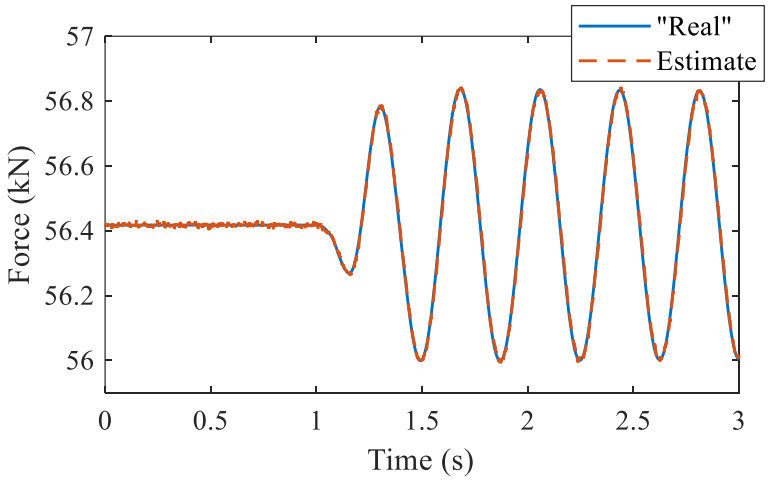

Figure 5: Comparison between the "real" and estimated contact force using only the car body acceleration measurement with 5% measurement noise ($v = 250$km/h).

forces using acceleration measurements from the car body with 5% measurement noise. The estimated contact force is close to the actual contact force acting on the vehicle, indicating that the vehicle speed has no effect on the performance of the AKF in contact force estimation, at least for the cases examined.

5.2 2-DOF vehicle with small wheel mass on a rail with irregularity

This section focuses on the same 2-DOF vehicle with a small wheel mass moving on the bridge at constant speed $v = 250$km/h. A "good quality" rail irregularity is present on the bridge only (i.e., there is no irregularity outside the bridge). This enables the evaluation of the performance of AKF in contact force estimation under different rail irregularity profiles. The covariance of the state error Q_x, the covariance of the measurement error Q_y, and the selection criteria of the covariance for the random walk model Q_λ remain the same as in the previous section.

Figure 6 compares the "real" and the estimated contact force using the car body acceleration measurement with the presence of 5% measurement noise. The method precisely captures the change in contact force due to the change in rail profile at $t = 1$s. Also, the method can capture

3, 250km/h

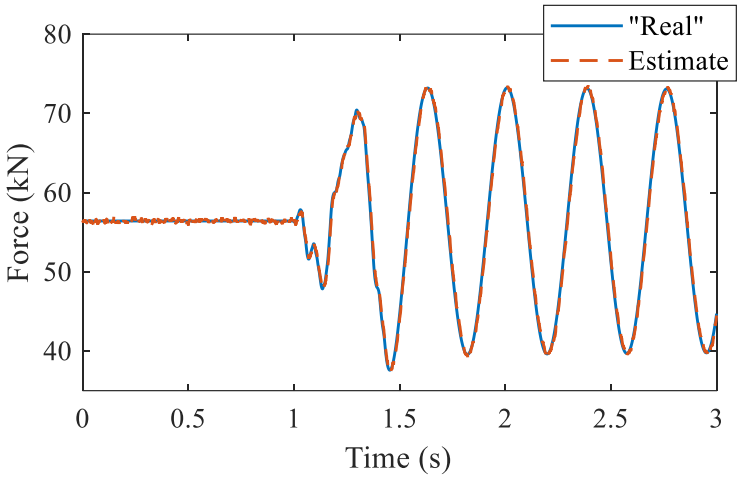

Figure 6: Comparison between the "real" and estimated contact force using only the car body acceleration measurement with 5% measurement noise ($v = 250$km/h) ("good quality" rail irregularity on the bridge).

the contact force fluctuation around the vehicles self-weight after the bridge with excellent accuracy. This demonstrates the effectiveness of the AKF in estimating the contact force of the vehicle under different rail profiles at high speed using solely vehicle measurement.

5.3 2-DOF vehicle with regular wheel mass on a rail with irregularity

To evaluate the effectiveness of the proposed method on a more realistic vehicle, we adjust the ratio of the wheel mass to the car body mass to match that of an actual vehicle. Table 3 shows the mechanical parameters of the vehicle. The vehicle moves on the bridge at constant speed $v = 250$km/h, and a "good quality" rail irregularity is present on the bridge only. The procedure of setting the covariance of the state error Q_x, the covariance of the measurement error Q_y, and the covariance for the random walk model Q_λ are the same as in Section 5.2.

Table 3: Mechanical properties of the 2-DOF vehicle with regular wheel mass.

m_c (t)	m_w (t)	k_p (MN/m)	c_p (kNs/m)
5.75	1	1.595	40

Figure 7 compares the "real" and the estimated contact force using the strain measurement at the suspension and acceleration measurement at the car body and wheel. Figure 7a shows that the AKF provides an accurate estimation of the contact force when there is no measurement noise. Even with the introduction of 5% measurement noise (Figure 7b), the AKF still provides a reliable estimation of the contact force. This demonstrates the effectiveness of the AKF in estimating the contact force of the vehicle in the presence of more realistic irregularity conditions.

5.4 Bridge Response Reconstruction

This section focuses on the reconstruction of the bridge response using the estimated contact force under the scenario of Section 5.3 (a 2-DOF vehicle moving at a constant speed $v =$

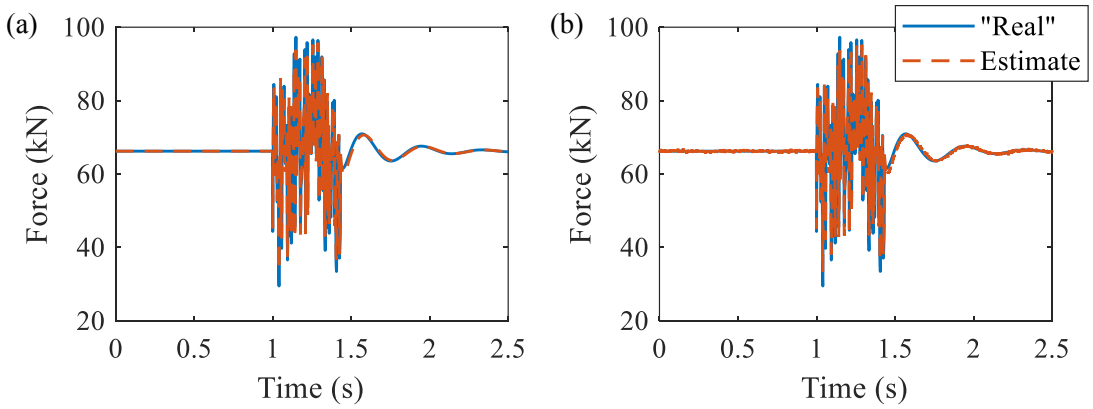

Figure 7: Comparison between the "real" and estimated contact force using the acceleration measurement at all DOF and the strain measurement at the suspension (a) without and (b) with

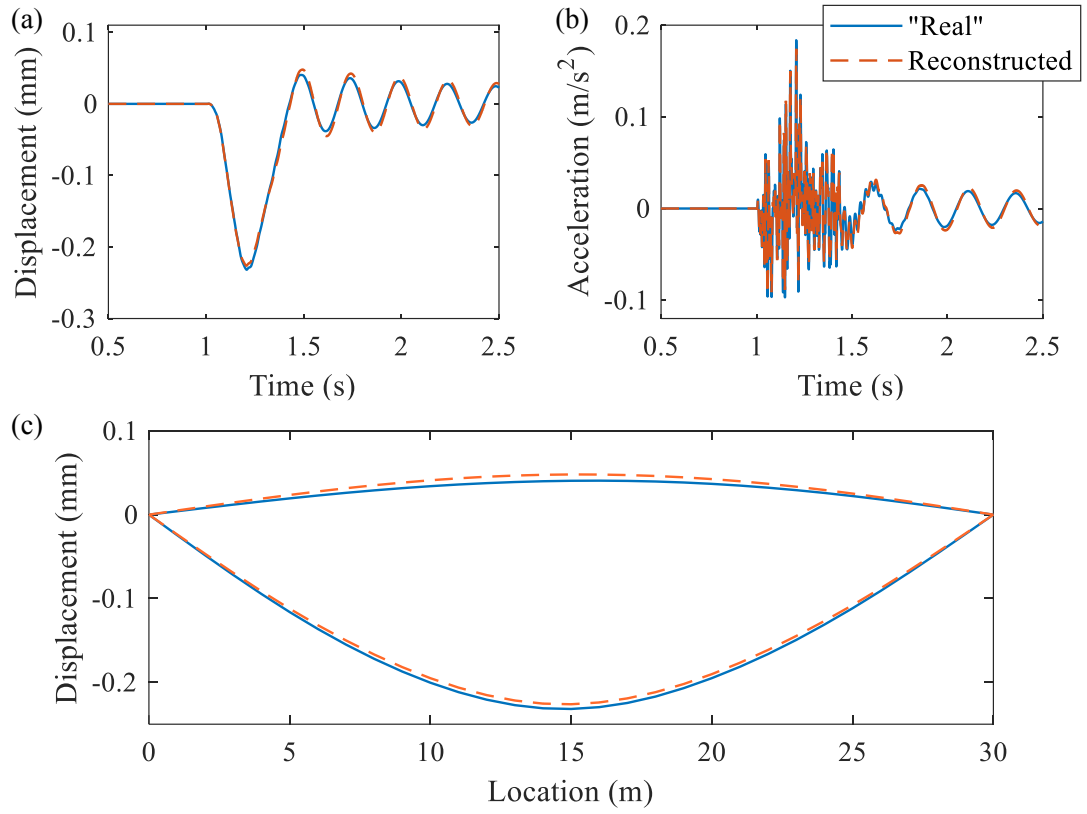

Figure 8: Comparison between the "real" and reconstructed (a) displacement response history, (b) acceleration response history at the midspan of the bridge, and (c) envelope of the deflection of the bridge ($v = 250$km/h) ("good quality" rail irregularity on the bridge).

Figure 8 compares the "real" response of the bridge (as calculated from the vehicle-bridge simulation) and the reconstructed bridge response using the estimated contact force. In particular, the reconstructed response is derived from the solutions of the EOM of the bridge (Eq. 2) using the estimated contact force from Section 5.3. This implies that we know the parameters of

the bridge model. The comparison is excellent in terms of displacement response history of the midspan of the bridge (Figure 8a), acceleration response history of the midspan of the bridge (Figure 8b), and very good in terms of the envelope deflection of the whole bridge (Figure 8c). These first results indicate that the proposed vehicle scanning approach with AKF estimation of the contact force can be promising for reconstructing the response of the bridge and hence useful for structural health monitoring applications.

6 CONCLUSIONS

This study examines the feasibility of identifying vehicle-bridge contact forces using solely measurements from on-board sensors (on vehicles). Specifically, it proposes the use of the Augmented Kalman Filter (AKF) for the identification of the unknown contact force acting on the vehicle. For the vehicle dynamics, the study assumes the vehicle is known, adopts mode superposition and formulates a state-space model of the vehicle, after removing the influence of the rigid body mode. In lieu of field measurements, to demonstrate the effectiveness and the performance of the AKF under different conditions, the analysis uses numerical simulation experiments. The vehicle-bridge simulation examines 2-DOF vehicle models at varying speeds and under different irregularities. The comparisons between the estimated and the "real" contact forces indicate that the AKF is capable of achieving high-accuracy contact force estimation with properly tuned covariance and sufficient measurement quantities. The analysis further demonstrates the accuracy of the bridge response reconstruction from the estimated contact force, assuming a known bridge model. Therefore, these first results illustrate the possibility of virtual sensing from on-board sensors and enhance the promise of the vehicle scanning (of bridges) approach.

7 ACKNOWLEDGEMENTS

Financial support to the second author was provided by the University Grants Committee Research Grants Council of Hong Kong, under Grant Reference Number GRF 16212522. Also, this project has received funding from the European Union's Horizon 2020 research and innovation programme under the Marie Skłodowska-Curie grant agreement No 764547 and from the General Secretariat of Research and Technology of Greece's Ministry of Education and Research.

REFERENCES

[1] Y. An, E. Chatzi, S.H. Sim, S. Laflamme, B. Blachowski, J. Ou, Recent progress and future trends on damage identification methods for bridge structures. *Structural Control and Health Monitoring* , **26**(10), 913–922, 2019.

[2] Y.B. Yang, C. Lin, J. Yau, Extracting bridge frequencies from the dynamic response of a passing vehicle. *Journal of Sound and Vibration*, **272**(3), 471-493, 2004.

[3] Y.B. Yang, J.P. Yang, B. Zhang, Y. Wu, Vehicle Scanning Method for Bridges. John Wiley Sons, Ltd, 2019.

[4] J. Li, X. Zhu, S. Law, B. Samali, Indirect bridge modal parameters identification with one stationary and one moving sensors and stochastic subspace identification. *Journal of Sound and Vibration*, **446**, 121, 2019.

[5] J. Zhan, J. You, X. Kong, N. Zhang, An indirect bridge frequency identification method using dynamic responses of high-speed railway vehicles. *Engineering Structures*, **243**, 112694, 2021.

[6] X. Jian, Y. Xia, L. Sun, An indirect method for bridge mode shapes identification based on wavelet analysis. *Structural Control and Health Monitoring*, **27**(12), e2630, 2020

[7] Y.B. Yang, W.F. Chen, H.W. Yu, C.S. Chan, Experimental study of a hand-drawn cart for measuring the bridge frequencies. *Engineering Structures* **57**, 222231, 2013.

[8] H. Xu, C.C. Huang, Z.L. Wang, K. Shi, Y.T. Wu, Y.B. Yang, Damped test vehicle for scanning bridge frequencies: Theory, simulation and experiment. *Journal of Sound and Vibration*, **506**, 116155, 2021

[9] Y.B. Yang, Y.H. Liu, D.Z. Guo, J.T. Zhou, Y.Z. Liu, H. Xu, Scanning the vertical and radial frequencies of curved bridges by a single-axle vehicle with two orthogonal degrees of freedom. *Engineering Structures*, **283**, 115939, 2023.

[10] Y.B. Yang, X.Q. Mo, K. Shi, Z.L. Wang, H. Xu, Y.T. Wu, Contact residue for simultaneous removal of vehicles frequency and surface roughness in scanning bridge frequencies using two connected vehicles. *International Journal of Structural Stability and Dynamics*, **21**(13), 2171006, 2021.

[11] Y.B. Yang, X.Q. Mo, K. Shi, Z.L. Wang, H. Xu, Y.T. Wu, Scanning torsional-flexural frequencies of thin-walled box girders with rough surface from vehicles residual contact response: Theoretical study. *Thin-Walled Structures*, **169**, 108332, 2021.

[12] E. Erduran, F. M. Pettersen, S. Gonen, A. Lau, Identification of vibration frequencies of railway bridges from train-mounted sensors using wavelet transformation. *Sensors*, **23**(3), 2023.

[13] N. Jin, Y.B. Yang, E.G. Dimitrakopoulos, T.S. Paraskeva, L.S. Katafygiotis, Application of short-time stochastic subspace identification to estimate bridge frequencies from a traversing vehicle. *Engineering Structures*, **230**, 111688, 2021.

[14] N. Jin, V.K. Dertimanis, E.N. Chatzi, E.G. Dimitrakopoulos, L.S. Katafygiotis, Subspace identification of bridge dynamics via traversing vehicle measurements. *Journal of Sound and Vibration*, **523**, 116690, 2022.

[15] A. Malekjafarian, E. OBrien, Identification of bridge mode shapes using short time frequency domain decomposition of the responses measured in a passing vehicle. *Engineering Structures* **81**, 386397, 2014.

[16] A. Malekjafarian, E. J. OBrien, On the use of a passing vehicle for the estimation of bridge mode shapes. *Journal of Sound and Vibration* **97**, 7791, 2017.

[17] J. Zhou, Z. Lu, Z. Zhou, C. Pan, S. Cao, J. Cheng, J. Zhang, Extraction of bridge mode shapes from the response of a two-axle passing vehicle using a two-peak spectrum idealized filter approach. *Mechanical Systems and Signal Processing* **190**, 110122, 2023.

[18] S. S. Eshkevari, T. J. Matarazzo, S. N. Pakzad, Bridge modal identification using acceleration measurements within moving vehicles. *Mechanical Systems and Signal Processing* **141**, 106733, 2020.

[19] S. S. Eshkevari, S. N. Pakzad, M. Tak, T. J. Matarazzo, Modal identification of bridges using mobile sensors with sparse vibration data. *Journal of Engineering Mechanics* **146**(4), 04020011, 2020.

[20] H. Ngwangwa, P. Heyns, F. Labuschagne, G. Kululanga, Reconstruction of road defects and road roughness classification using vehicle responses with artificial neural networks simulation. *Journal of Terramechanics* **47**(2), 97111, 2010.

[21] H. Ngwangwa, P. Heyns, Application of an ANN-based methodology for road surface condition identification on mining vehicles and roads. *Journal of Terramechanics*, **53**, 5974, 2014.

[22] Q. Zeng, X. Hu, X. Shi, Y. Ren, Y. Li, Z. Duan, Estimation of road roughness based on tire pressure monitoring. *International Journal of Structural Stability and Dynamics*, **22**(06), 2250073, 2022.

[23] B. Zhao, T. Nagayama, K. Xue, Road profile estimation, and its numerical and experimental validation, by smartphone measurement of the dynamic responses of an ordinary vehicle. *Journal of Sound and Vibration* **457**, 92117, 2019.

[24] K. Xue, T. Nagayama, B. Zhao, Road profile estimation and half-car model identification through the automated processing of smartphone data. *Mechanical Systems and Signal Processing*, **142**, 106722, 2020.

[25] Y. He, J. P. Yang, Using Kalman filter to estimate the pavement profile of a bridge from a passing vehicle considering their interaction. *Acta Mechanica*, **232**(11), 43474362, 2021.

[26] X. Xiao, X. Xu, W. Shen, Identification of frequencies and track irregularities of railway bridges using vehicle responses: A Recursive Bayesian Kalman Filter Algorithm. *Journal of Engineering Mechanics* **148**(9), 04022051, 2022.

[27] E. Lourens, E. Reynders, G. De Roeck, G. Degrande, G. Lombaert, An augmented Kalman filter for force identification in structural dynamics. *Mechanical Systems and Signal Processing*, **27**(1), 446-460, 2012.

[28] S. Eftekhar Azam, E. Chatzi, C. Papadimitriou, A dual Kalman filter approach for state estimation via output-only acceleration measurements. *Mechanical Systems and Signal Processing*, **60**, 866886, 2015.

[29] Y. Lei, D. Xia, K. Erazo, S. Nagarajaiah, A novel unscented Kalman filter for recursive state-input-system identification of nonlinear systems. *Mechanical Systems and Signal Processing*, **127**, 120135, 2019.

[30] Z. Chen, Z. Xie, J. Zhang, Measurement of vehicle-bridge-interaction force using dynamic tire pressure monitoring. *Mechanical Systems and Signal Processing*, **104**, 370383, 2018.

[31] H. Wang, T. Nagayama, D. Su, Estimation of dynamic tire force by measurement of vehicle body responses with numerical and experimental validation. *Mechanical Systems and Signal Processing*, **123**, 369385, 2019.

[32] C.D. Stoura, E.G. Dimitrakopoulos, Additional damping effect on bridges because of vehicle-bridge interaction. *Journal of Sound and Vibration* **476**, 115294, 2020.

[33] C.D. Stoura, E.G. Dimitrakopoulos, MDOF extension of the Modified Bridge System method for vehiclebridge interaction. *Nonlinear Dynamics*, **102**, 2103-2123, 2020.

[34] E.G. Dimitrakopoulos, Q. Zeng, A three-dimensional dynamic analysis scheme for the interaction between trains and curved railway bridges. *Computers and Structures*, **149**, 4360, 2015.

[35] Y.B. Yang, J.D. Yau, Y.S. Wu, Vehicle-Bridge Interaction Dynamics: With Applications to High-Speed Railways. World Scientific, 2004.

[36] W. Guo, H. Xia, G. De Roeck, K. Liu, Integral model for train-track-bridge interaction on the Sesia viaduct: Dynamic simulation and critical assessment. *Computers and Structures*, **112-113**, 205-216, 2012.